

# Self-supervised Learning of Event-guided Video Frame Interpolation for Rolling Shutter Frames

Yunfan Lu<sup>1</sup>\* Guoqiang Liang<sup>1</sup>\* Lin Wang<sup>1,2†</sup>

<sup>1</sup>VLIS LAB, AI Thrust, HKUST(GZ) <sup>2</sup>Dept. of Computer Science and Engineering, HKUST  
 {yly066, gliang041}@connect.hkust-gz.edu.cn, linwang@ust.hk

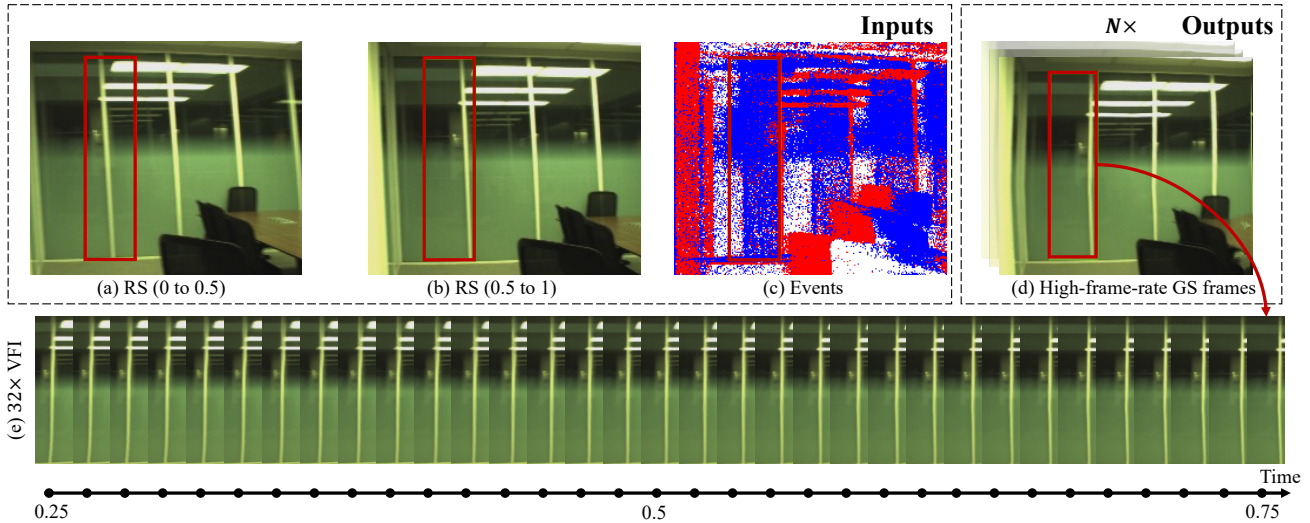


Figure 1: We propose a novel VFI method that enables the recovery of in-between GS frames (d) with an arbitrary frame rate from two consecutive RS frames (a and b), guided by the novel event camera data (c) in a *self-supervised manner*. Here, 0 - 0.5 and 0.5 - 1 are the normalized exposure time. Importantly, our method can achieve a significant temporal resolution up to  $32 \times$  frame rate (e).

## Abstract

This paper makes the **first** attempt to tackle the challenging task of recovering arbitrary frame rate latent global shutter (GS) frames from two consecutive rolling shutter (RS) frames, guided by the novel event camera data. Although events possess high temporal resolution, beneficial for video frame interpolation (VFI), a hurdle in tackling this task is the lack of paired GS frames. Another challenge is that RS frames are susceptible to distortion when capturing moving objects. To this end, we propose a novel self-supervised framework that leverages events to guide RS frame correction and VFI in a unified framework. Our key idea is to estimate the displacement field (**DF**)—non-linear dense 3D spatiotemporal information of all pixels during the exposure time, allowing for the reciprocal reconstruction between RS and GS frames as well as ar-

bitrary frame rate VFI. Specifically, the displacement field estimation (DFE) module is proposed to estimate the spatiotemporal motion from events to correct the RS distortion and interpolate the GS frames in one step. We then combine the input RS frames and DF to learn a mapping for RS-to-GS frame interpolation. However, as the mapping is highly under-constrained, we couple it with an inverse mapping (*i.e.*, GS-to-RS) and RS frame warping (*i.e.*, RS-to-RS) for self-supervision. As there is a lack of labeled datasets for evaluation, we generate two synthetic datasets and collect a real-world dataset to train and test our method. Experimental results show that our method yields comparable or better performance with prior supervised methods.

## 1. Introduction

CMOS cameras are dominantly applied to consumer-grade devices, *e.g.*, mobile phones, due to their low cost and power consumption [8, 3, 16, 36]. These sensors, how-

\*These authors are co-first authors.

†Corresponding author

ever, struggle with the rolling shutter (RS) effect, leading to unexpected distortion problems, *e.g.*, skew, when capturing fast-moving objects. By contrast, global shutter (GS) sensors synchronize the exposure period of all pixels; therefore, they do not suffer from edge distortion and region occlusion [26, 8, 5, 14, 23]. With the growing demand for high frame rate and high-quality videos for mobile devices, deep learning-based video frame interpolation (VFI) has attracted increasing attention in the research community [18, 41]. Despite the success of these VFI methods [25, 18, 27, 42, 28, 2, 32, 30], they all follow the GS mechanism. Therefore, they often fail to recover latent GS frames from two consecutive RS frames, captured by the RS sensors, especially, the high-speed or dynamic motion scenes [38]. To tackle this problem, many learning-based RS correction methods [24, 34, 47] have been proposed to obtain GS frames by removing the RS effect based on the assumption of linear motion. However, they can not synthesize nonexistent in-between GS frames. Therefore, it is desirable to generate in-between GS frames from two consecutive RS frames as it can benefit both VFI and RS correction. Accordingly, some learning-based methods have been proposed. RSSR [5] and CVR [8] are two representative methods that estimate the linear motion to recover faithful in-between GS frames from two consecutive RS frames. However, they can not handle non-linear motion, which often occurs in dynamic scenes with fast motion.

Event cameras are bio-inspired sensors that can asynchronously detect per-pixel intensity changes and generate event streams with high temporal resolution—*1us* and high dynamic range compared with the frame-based cameras—*140dB* vs. *60dB* [35, 9, 45]. This has inspired some research endeavors [38, 37, 15, 29, 43, 41], exploring event streams as the guidance to compensate for motion information loss for VFI in the dynamic scenes with fast motion. However, these methods only serve the goal of GS frame interpolation via supervised learning. Moreover, they necessitate paired GS and RS frame data, which are typically acquired via simulation on high-speed videos [8, 5]. This not only incurs substantial costs but also restricts the practical usage of these techniques in real-world scenarios.

In this paper, we make the **first** attempt to *leverage the high temporal resolution of events to guide the recovery of in-between GS frames from two consecutive RS frames*. However, tackling this novel problem is non-trivial because 1) there do not exist GS-events-RS triplet datasets for VFI, and 2) RS frames are susceptible to edge distortion and region occlusion in dynamic scenes with fast motion. To this end, we propose a novel *self-supervised learning* (SSL) framework that leverages events to guide RS correction and VFI in a unified framework. Overall, our method enables the recovery of GS frames with *any arbitrary frame rate*, *e.g.*,  $32\times$ , from two consecutive RS frames, guided by

events, as depicted in Fig. 1. The proposed SSL framework is shown in Fig. 2. The key idea of our method is to 1) estimate the 3D *displacement field* (DF), which includes dense spatiotemporal non-linear motion information of all pixels during the exposure time, and 2) combine the RS frames and DF for the reciprocal reconstruction (or mapping) to impose self-supervision.

Specifically, we first propose the displacement field estimation module to estimate the spatiotemporal motion information from events directly (Sec. 4.1). We split events into moments, each of which includes a fixed amount of voxel grid [33, 11]. We estimate the optical flow [12] between consecutive event moments. This way, we can obtain the non-linear 3D motion information—DF, during the exposure time for GS frames. Benefiting from the high temporal resolution of events, 3D DF contains dense motion information for RS correction and GS frames interpolation in one step. Based on DF, we propose a latent GS frames generation module to learn the RS-to-GS mapping for GS frame interpolation (Sec. 4.2). We generate a series of GS frames at arbitrary frame rate in exposure time from RS frames and 3D DF. As the ground truth GS frames are not available, the mapping is highly under-constrained. Thus, we couple it with a reciprocal reconstruction module to 1) reconstruct RS frames based on the generated GS frames and fully exploit the constraints inherent in RS frames, and 2) achieve RS-to-RS warping based on the DF for self-supervision (Sec. 4.3).

Due to the lack of RS-events-GS triplet datasets, we generate two simulated datasets for qualitative and quantitative evaluation. Moreover, we collect a real-world dataset with RS frames and aligned events for training and qualitative assessment of our SSL method. Experimental results show that our method yields **1) comparable** performance with supervised frame-based RS-to-GS VFI method [8] and **2) better** performance than the supervised event-guided RS correction [46] + unsupervised event-guided VFI method—TimeReplayer [15]. Note that with RS frames and events as inputs, our method achieves much higher VFI performance than that of TimeLens (only for GS frames) [38]. In summary, the contributions of this paper are four-fold: **(I)** we make the *first* attempt to address GS frame VFI from RS frames, guided by events. **(II)** We propose an SSL framework that can generate arbitrary frame rate GS frames from RS frames and events. **(III)** We introduce a DF estimation module and a reciprocal reconstruction module to impose self-supervision. **(IV)** We introduce two synthetic and one real-world datasets for the training and evaluation.

## 2. Related Works

**Event-guided VFI:** Video frame interpolation (VFI) is a fundamental task converting low frame rate videos to high frame rate videos in video enhancement [25, 4, 31]. Dur-

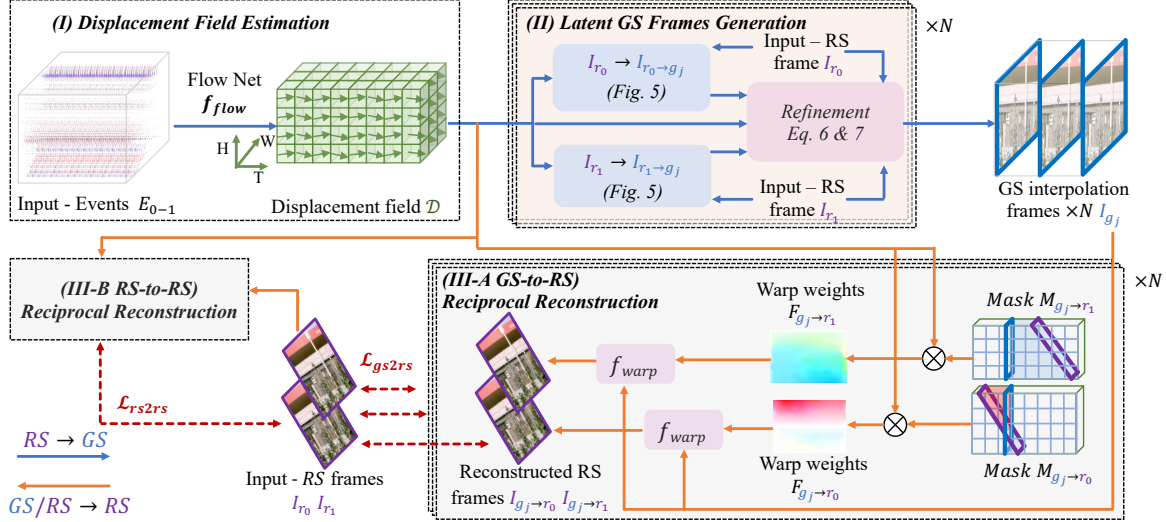


Figure 2: Overview of our proposed framework, which consists of three parts, the displacement field estimation module, latent GS frames generation module, and the reciprocal reconstruction module. See contexts for more details.

Methods	Event Based	Self Supervised	Rolling Correction	Frame Interpolation
EvUnroll [46]	✓	✗	✓	✗
TimeReplayer [15]	✓	✓	✗	✓
TimeLens [38]	✓	✗	✗	✓
RSSR [5]	✗	✗	✓	✓
CVR [8]	✗	✗	✓	✓
<b>Ours</b>	✓	✓	✓	✓

Table 1: Comparison of our method with prior-arts.

ing generating intermediate frames between consecutive frames, frame-based methods [25, 18, 27, 42, 28, 2, 32, 30] predict motion explicitly or implicitly. However, these methods degrade greatly in scenes of non-linear motion since accurately modeling motion from the sparse set of frames is ill-posed [43]. Unlike the RGB camera, event camera enjoys many advantages, such as high temporal resolution, which captures the brightness changes in a time interval [38]. Previous works have demonstrated its potential for VFI, and they can be roughly categorized into two types: supervised and unsupervised methods. The supervised methods can also be divided into two parts: synthesis-based and wrapping-based methods. For example, EFI [29], is a synthesis-based method that generates intermediate frames from events and images.  $A^2OF$  [41] explores the relation between event counts and motion, and designs event-driven optical flow masks for warping intermediate frames. Time Lens [38] and Time Lens++ [37] combine synthesis methods with warping-based methods to boost the VFI performance. TimeReplayer [15] is an unsupervised approach that applies a loss between the input frames and recon-

structed input frames—warped from interpolated frames. All these methods are designed for the GS frames without considering the distortion caused by RS. However, most commercial cameras record frames with the RS mechanism, thus impeding their applications in real-world scenarios.

**RS correction:** Recently, some learning-based methods [24, 6, 7, 1, 8] have been proposed to achieve the RS correction. As the motion information between frames is unknown, these methods rely on the prior assumption of linear motion to predict the intermediate GS frames, which degrade greatly in scenes of non-linear motion. Zhou *et al.* [46] explored the spatiotemporal information of event cameras to boost the performance of RS correction with the non-linear motion for the target time. However, they focus on RS correction and deblurring without considering RS-to-GS frame interpolation.

**VFI with RS frames:** RSSR [5] proposes the first work to recover a random frame rate GS frame from RS frames, while the results suffer from unwanted holes and black edges, caused by occlusion between the RS and GS frames. CVR [8] then proposes a context-aware GS frame interpolation framework to alleviate the occlusion problem and reduce artifacts. However, these methods are frame-based and only focus on linear motion. It is demanding to consider non-linear motion for real-world applications. In addition, these methods need the paired RS-GS dataset for training, which is difficult to collect. Therefore, they only conduct experiments on the synthetic dataset. We make the first attempt to leverage events to guide RS correction and VFI in one step, as shown in Tab. 1. Accordingly, we propose a self-supervised approach that generates the arbi-

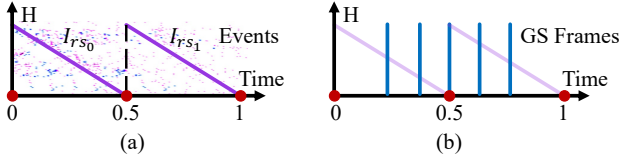


Figure 3: Illustration of the input RS frames (purple) and events (a) and output GS frames after interpolation (blue) for  $4 \times$  VFI (b).

bitrary frame rate GS frames between consecutive RS frames.

### 3. Preliminaries

Rolling Shutter is an exposure mechanism widely deployed in commercial cameras, which determines the VFI problem definition. First, we denote  $\mathbf{L}$  as the intensity of an ideal video sequence in the period of  $[t_s, t_e]$  containing continuous GS frames. A RS frame  $I_r$  can be regarded as a special composition of a series of GS frames. We denote the  $t_s^r$  and  $t_e^r$  as the start and end of the exposure time of RS frame  $I_r$ , respectively. The interval of exposure time between every two adjacent lines is  $\Delta t = (t_s^r - t_e^r)/(H - 1)$ , where  $H$  is the height of video frames. Therefore, the exposure time of row  $h$  of the RS frame can be recorded as  $t_h = t_s^r + h \times \Delta t$ . Then the raw  $h$  of RS frame  $I_r$  can be formulated as Eq. 1, where  $I_{t_h}[h]$  refers to the row  $h$  of the GS frame captured at  $t_h$ .

$$I_{rs}[h] = I_{t_h}[h]. \quad (1)$$

For an event stream  $E$ , which is a set of event  $e = \{(t, x, y, p)\}$ , each event is triggered and recorded when the brightness change exceeds a certain threshold  $C$  at pixel  $(x, y)$ . Denote the time interval as  $\Delta t_e$ , which is quite a short period, and the brightness at position  $(x, y)$  as  $\mathbf{L}(t, x, y)$ , where  $x \in [0, H]$  and  $y \in [0, W]$ . The brightness change can be calculated as  $\Delta b = \log(\mathbf{L}(t_e, x_e, y_e)) - \log(\mathbf{L}(t_e - \Delta t_e, x_e, y_e))$ . Hence, the event at  $t$  can be formulated as  $p_e = \Phi(\Delta b, C)$ , where  $\Phi$  is the event triggering function. Event is recorded when  $|\Delta b| > C$ , and  $p_e \in \{1, -1\}$  indicates the increase or decrease.

### 4. Proposed Framework

**Overview:** The overall framework of the proposed approach is depicted in Fig. 2, which can be divided into three parts: (I) Displacement Field Estimation, (II) Latent GS frames Generation, and (III) Reciprocal Reconstruction. As the oversimplified linear motion model fails in complex non-linear motions, we first introduce DF which contains non-linear motion during the exposure time and bridge the gap between RS frames and GS frames (Sec. 4.1), followed by describing how to generate latent GS frames by RS frames and DF (Sec. 4.2). Since the mapping from RS to

GS is highly under-constrained, we couple it with the inverse mapping (GS-to-RS) and RS frame warping (RS-to-RS) for self-supervision (Sec. 4.3). The inputs of our framework are two consecutive RS frames ( $I_{r_0}, I_{r_1}$ ) and their corresponding events, while the outputs are continuous latent global shutter (GS) frames at arbitrary frame rate, as shown in Fig. 3.

#### 4.1. Displacement Field Estimation (DFE)

This module aims to model non-linear motion information from events and lays a foundation for reciprocal reconstruction between GS and RS frames. Assume that the camera captures a 3D point in complex non-linear motion, and the trajectory of this point in the exposure time is denoted as  $tr(t) = (x, y)$ , where  $t$  is the timestamp and  $(x, y)$  is the pixel location. Due to the non-linear character of  $tr$ , it can not be accurately expressed using previous frame-based VFI methods based on the assumption of linear motion [5, 8]. To this end, we decompose the whole trajectory into several pieces and use a piece-wise linear function to fit it. Given a very short time period  $[t_0, t_1]$ , the pixel location  $p_{t_0}$  and  $p_{t_1}$  at these two timestamps are  $tr(t_0) = (x_0, y_0)$  and  $tr(t_1) = (x_1, y_1)$ , respectively. We use linear approximation to fit the motion during  $t_0 - t_1$ , then we can obtain  $\Delta p_{0 \rightarrow 1} = tr(t_1) - tr(t_0) = (x_1 - x_0, y_1 - y_0)$ , which is the displacement from time  $t_0$  to time  $t_1$ .  $\Delta p_{0 \rightarrow 1}$  can be easily approximated by the estimation of the optical flow. However, how to estimate the optical flow in a small time period  $[t_0, t_1]$  is challenging.

To address this issue, we leverage the high-temporal resolution of events to estimate the optical flow within  $[t_0, t_1]$ . We divide the events into  $T + 1$  time bins, and each time bin is further divided into  $N$  voxel grids [33, 39]. Based on this, we can get the event representation with a dimension of  $(T + 1) \times N \times H \times W$ . We denote the event-based optical flow estimation function as  $f_{flow}$ , and the dimension of the estimated optical flow set is  $2 \times T \times H \times W$ . In practice, we estimate a set of optical flows as the DF— $\mathcal{D}$  by E-RAFT [12], as it has shown promising results in handling challenging motion scenes. In this way, we can fit the nonlinear motion with the linear motions of  $T$  segments. If we know the location of a pixel at time  $t_0$  and there is a considerable time gap between  $t_0$  and  $t_n$ , we can obtain the location of this point at time  $t_n$  by adding up its displacement in DF over the time interval, as Eq. 2.

$$\begin{aligned} tr(t_n) &= tr(t_0) + \sum_{i=1}^n (tr(t_i) - tr(t_{i-1})) \\ &= tr(t_0) + \sum_{i=1}^n p_{i-1 \rightarrow i}. \end{aligned} \quad (2)$$

**Displacement field Loss:** To encourage generating a smooth displacement field, we follow previous works [15,



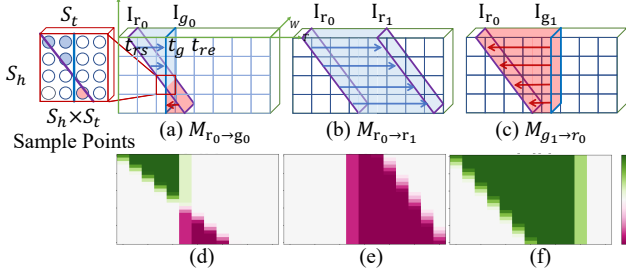


Figure 4: An illustration of masks of RS-to-GS and RS-to-RS for the displacement field. **Blue** represents a positive value, indicating forward movement. **Red** represents a negative value, indicating backward movement. Each item in the mask uses uniform sample  $S_h \times S_t$  points to estimate its weight. (a) shows more detail. Two-time points control the rolling shutter frame, the start exposure time  $t_{rs}$  and the end exposure time  $t_{re}$ . The global shutter frame is controlled by the exposure time  $t_g$ . (d) (e) (f) shows the projection of different masks on the  $H \times T$  dimension. For example, (d) shows the transition from rolling shutter frame (*start exposure time 0 and end exposure time 0.7*) to global shutter frame (*exposure time 0.4*).

[18] to promote the consistency in flow values between adjacent pixels, as in Eq. 3, where  $\nabla$  is a directional gradient and  $T$  is the temporal dimension.

$$\mathcal{L}_{field} = \frac{1}{T} \sum_{i=1}^T ((\nabla_x \mathcal{D}[i])^2 + (\nabla_y \mathcal{D}[i])^2) \quad (3)$$

**Mask Design for RS GS transformation** We designed the mask based on the exposure mechanism of the rolling shutter and global shutter to describe the transition between any two frames. The real exposure model of the rolling shutter frame and events are shown in Fig.4. The red solid line represents the start time of the frame exposure, and the red dashed line represents the end time of the frame exposure. It can be easily found that the exposure time is much shorter than the rolling shutter time. Long exposure time can lead to blurring, which complicates the research question of frame interpolation, and we do not consider the long exposure in the paper. Therefore, we approximate the rolling shutter frame and the global shutter frame as planes. Obviously, the plane of the global shutter can be described as  $t = t_g$ , where  $t_g$  is the global shutter exposure timestamp. The plane of the rolling shutter is parallel to the W-axis and passes through two points  $(h, t_{rs})$  and  $(0, t_{re})$  at the same time, where  $h$  is the height of frames, and  $t_{rs}$  and  $t_{re}$  are begin time and end time of rolling shutter frame exposure.

Given two planes, we use uniform sampling to calculate the weights of each bin in each mask. For each sampling point, we calculate whether it is on the left or right of the plane by computational geometry. Fig.4 shows the projec-

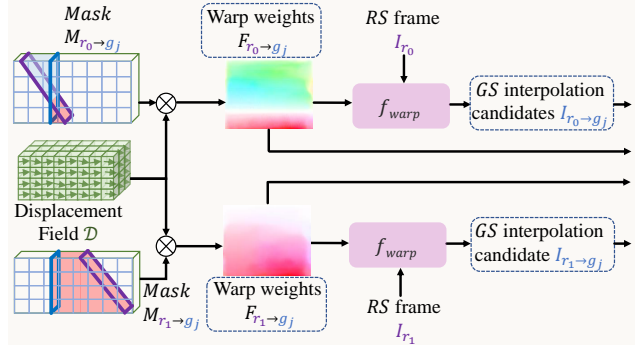


Figure 5: The illustration of latent GS generation from RS frames  $I_{r_0}$ ,  $I_{r_1}$  and displacement field  $\mathcal{D}$ . The dash boxes indicate the output.

tion of more masks in the  $H \times T$  dimension.

## 4.2. Latent Global Shutter Frame Generation

This module aims to generate a series of latent GS frames based on RS frames and DF, as shown in Fig 2 (II).Based on the analysis in Sec. 4.1, it can be inferred that the value of any point in the video can be determined by the value of a known point and the corresponding transformation in the  $\mathcal{D}$ .Therefore, masks are proposed to select the corresponding displacement field information for the reciprocal reconstruction between RS and GS frames, as shown in Fig. 4. The shape of the mask is  $T \times H \times W$ , and each item of the mask is a weight of motion for the corresponding position in DF. Specifically, we represent RS or GS frames as planes determined by their exposure time. We sample uniformly inside each item in the mask, and for each sampled point we calculate its direction to the RS and GS planes, as shown in Fig.4.For example, Fig. 4 (a) shows the mask  $\mathcal{M}_{r_0 \to g_0}$  of RS frame  $I_{r_0}$  to GS frame  $I_{g_0}$ . Blue and red indicate the forward and backward deformation from  $I_{r_0}$  to generate  $I_{g_0}$ .

We denote the mask that converts the  $i$ -th RS frame  $I_{r_i}$  into the  $j$ -th GS frame  $I_{g_j}$  as  $\mathcal{M}_{r_i \to g_j}$ . For the generation of GS frames, we use the Eq. 4 and Eq. 5, where  $f_{warp}$  is the warping function [13],  $F_{r_0 \to g_j}$  and  $F_{r_1 \to g_j}$  are warp weights for  $I_{r_0}$  and  $I_{r_1}$  to  $I_{g_j}$ ,  $I_{r_i \to g_j}$  is the  $j$ -th GS frame reconstructed from  $i$ -th RS frame, and  $\otimes$  denotes the dot product and sum in the temporal dimension.

$$F_{r_0 \to g_j} = \mathcal{D} \otimes \mathcal{M}_{r_0 \to g_j}, F_{r_1 \to g_j} = \mathcal{D} \otimes \mathcal{M}_{r_1 \to g_j}, \quad (4)$$

$$I_{r_i \to g_j} = f_{warp}(I_{r_i}, F_{r_i \to g_j}), i = \{0, 1\} \quad (5)$$

This way, we can predict an arbitrary number of GS frames from two input RS frames, respectively, as shown in Fig. 2(II). However, due to the occlusions and viewing angles, the quality of the GS frame mapped from a

single RS frame is not good enough; therefore, we propose a refine network  $f_{refine}$  to fuse multiple GS frames. For convenience, we employ U-Net, used by CVR [8], as the refined network. Specifically, we concatenate the  $I_{r_0}, I_{r_1}, I_{r_0 \rightarrow gi}, I_{r_1 \rightarrow gj}, F_{r_1 \rightarrow gj}$ , and  $F_{r_0 \rightarrow gj}$  in the channel dimension, so that the network can obtain RS frames and motion information from different perspectives, and fusion to reduce the occlusion effect. The input and output of  $f_{refine}$  are formulated in Eq. 6,

$$\begin{aligned} & \Delta F_{r_0 \rightarrow gj}, \Delta F_{r_1 \rightarrow gj}, O_{gj} = \\ & f_{refine}(I_{r_0 \rightarrow gj}, I_{r_1 \rightarrow gj}, I_{r_0}, I_{r_1}, F_{r_0 \rightarrow gj}, F_{r_1 \rightarrow gj}), \end{aligned} \quad (6)$$

where  $\Delta F_{r_0 \rightarrow gj}, \Delta F_{r_1 \rightarrow gj}$  are residuals of the warp weights  $F_{r_0 \rightarrow gj}$  and  $F_{r_1 \rightarrow gj}$ , and  $O_{gj} \in [0, 1]$  is the degree of occlusion for  $I_{r_0}$ . Therefore, the refined latent  $j$ -th GS frame is generated, as formulated in Eq. 7:

$$\begin{aligned} I_{gj} = & O_{gj} \times f_{warp}(I_{r_0}, F_{r_0 \rightarrow gj} + \Delta F_{r_0 \rightarrow gj}) + \\ & (1 - O_{gj}) \times f_{warp}(I_{r_1}, F_{r_1 \rightarrow gj} + \Delta F_{r_1 \rightarrow gj}). \end{aligned} \quad (7)$$

### 4.3. Reciprocal Reconstruction

As the ground truth GS frames are not available and the mapping from the input RS frames to latent GS frames is highly under-constrained, this module exploits how to reconstruct RS frames from a single GS frame for the purpose of self-supervision. As the displacement field includes the non-linear dense 3D spatiotemporal information of all pixels during the exposure time, we can simply achieve this target by Eq. 8 and Eq. 9, where  $\mathcal{M}_{g_j \rightarrow r_i}$  is the mask from  $j$ -th GS frame  $I_{g_j}$  to  $i$ -th RS frame  $I_{r_i}$ . Based on the definition of mask in Sec. 4.1, it indicates that masks of RS-to-GS and GS-to-RS are reversible for each other, namely  $\mathcal{M}_{g_j \rightarrow r_i} = -\mathcal{M}_{r_i \rightarrow g_j}$ . Because we can reconstruct RS frames  $I_{r_0}$  or  $I_{r_1}$  from each predicted latent GS frame  $I_{g_j}$ , we convert the supervision from the reconstruction of latent GS frames to the reconstruction of input RS frame.

$$\begin{aligned} F_{g_j \rightarrow r_0} &= \mathcal{D} \otimes \mathcal{M}_{g_j \rightarrow r_0}, \\ F_{g_j \rightarrow r_1} &= \mathcal{D} \otimes \mathcal{M}_{g_j \rightarrow r_1} \end{aligned} \quad (8)$$

$$I_{g_j \rightarrow r_i} = f_{warp}(I_{g_j}, F_{g_j \rightarrow r_i}), i = \{0, 1\} \quad (9)$$

**(A) GS-to-RS Loss:** To realize the self-supervision, we reconstruct the input RS frames  $I_{r_0}, I_{r_1}$  from the generated  $i$ -th frame  $I_{g_i}$ . For simplicity, we use the *Charbonnier loss*  $\mathcal{L}_c$  [22] as the GS-to-RS self-supervision loss, formulated as:

$$\mathcal{L}_{gs2rs} = \frac{1}{2N} \sum_{i=1}^N (\mathcal{L}_c(I_{g_i \rightarrow r_0}, I_{r_0}) + \mathcal{L}_c(I_{g_i \rightarrow r_1}, I_{r_1})), \quad (10)$$

where  $N$  is the number of predicted GS frames.

**(B) RS-to-RS Loss:** Since the two input RS frames have spatiotemporal coherence, we leverage it as the constraint

for imposing additional self-supervision. We reconstruct  $i$ -th RS frame by warping  $j$ -th RS frame and displacement field as Eq. 11 and Eq. 12. Then, we employ the  $\mathcal{L}_c$  as our RS-to-RS loss as Eq. 13.

$$I_{r_1 \rightarrow r_0} = f_{warp}(I_{r_1}, (\mathcal{D} \otimes \mathcal{M}_{r_1 \rightarrow r_0})), \quad (11)$$

$$I_{r_0 \rightarrow r_1} = f_{warp}(I_{r_0}, (\mathcal{D} \otimes \mathcal{M}_{r_1 \rightarrow r_0})), \quad (12)$$

$$\mathcal{L}_{rs2rs} = \mathcal{L}_c(I_{r_0 \rightarrow r_1}, I_{r_1}) + \mathcal{L}_c(I_{r_1 \rightarrow r_0}, I_{r_0}) \quad (13)$$

**Total Loss:** Finally, the total loss can be summarized as Eq. 14, where  $\lambda_f, \lambda_{rs}, \lambda_{gs}$  denote the weights of each loss.

$$\mathcal{L} = \lambda_f \mathcal{L}_{field} + \lambda_{rs} \mathcal{L}_{rs2rs} + \lambda_{gs} \mathcal{L}_{gs2rs} \quad (14)$$

## 5. Experiments

**Implementation Details:** We employ the Adam optimizer [20] for all experiments, with learning rates of  $1e-4$  for Gev-RS, Fastec-RS and E-RS-VFI datasets, respectively. Our framework is trained for 100 epochs with the batch size of 4 using an NVIDIA RTX A30 GPU.

**Evaluation Metrics:** We evaluate our approach using the peak-signal-to-noise ratio (PSNR) [17] and structural similarity (SSIM) [40] and perceptual similarity metric LPIPS [44].

**Dataset: 1) Gev-RS dataset** [46] provides original videos captured by GS high-speed cameras with  $1280 \times 720$  resolution at 5700 fps. Notably, EvUnroll [46] considers both RS correction and deblurring, thus their simulation dataset includes blurry frames and lacks high frame rate frames for VFI evaluation. Therefore, we reconstruct RS frames and events from original videos to avoid the influence of blurring. Because tackling deblurring, RS correction, and VFI is extremely challenging. We first downsample the original videos to the same resolution ( $260 \times 346$ ) of the DAVIS346 event camera [35]. Then, we input the resized frames to the event simulator vid2e [10] to synthesize event streams. We generate RS frames based on the same RS simulation process of Fastec-RS [24]. We follow the same dataset split scheme as in EvUnroll [46]: 20 videos for training and 9 videos for testing. **2) Fastec-RS dataset** Fastec-RS dataset [24] provides the original frame sequences which are recorded by the high-speed GS cameras with the resolution of  $640 \times 480$  at 2400 fps. We follow the aforementioned settings to downsample frame sequences and generate the corresponding event streams and RS frames. Besides, we employ the same dataset split scheme as in Fastec-RS [24]: 56 sequences for training and 20 sequences for testing. **3) ERS-VFI dataset** To evaluate our method on the real-world dataset, we use an ALPIX-Eiger event camera <sup>1</sup> to collect a new dataset, called

<sup>1</sup><https://www.alpsentek.com/product>

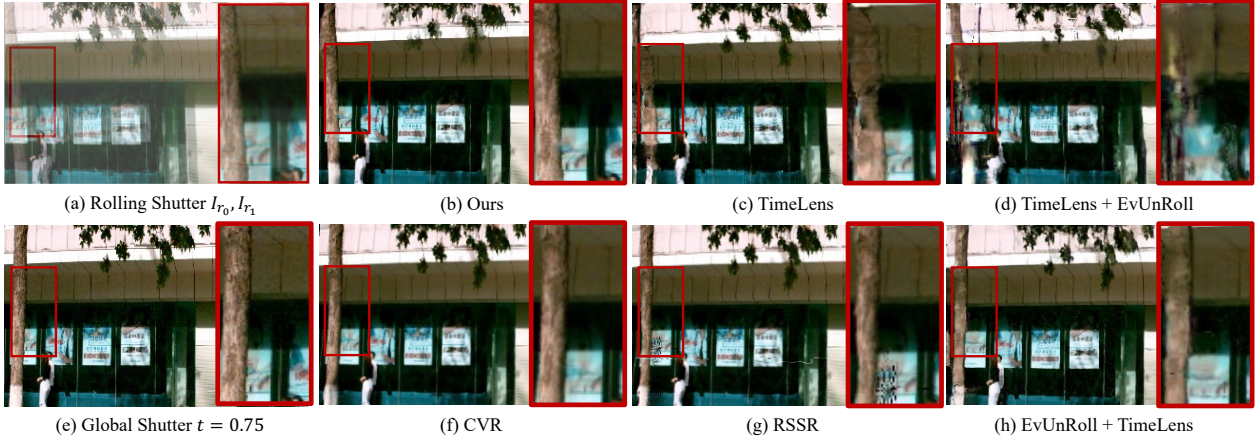


Figure 6: Visual comparison on Gev-RS dataset.

Methods	Params(M)	Event	SSL	4×	8×	16×	24×	32×
CVR[8]	42.69	✗	✗	22.59 / 0.7508 / 0.1094	23.80 / 0.7949 / 0.1027	24.60 / 0.8209 / 0.0990	24.85 / 0.8291 / 0.0979	24.98 / 0.8331 / 0.0973
RSSR[5]	26.04	✗	✗	17.83 / 0.5875 / 0.1498	17.58 / 0.5762 / 0.1532	17.45 / 0.5701 / 0.1553	17.40 / 0.5680 / 0.1560	17.37 / 0.5670 / 0.1562
TL[38]	72.20	✓	✗	19.77 / 0.6408 / 0.1563	19.86 / 0.6476 / 0.1518	19.88 / 0.6492 / 0.1506	19.90 / 0.6128 / 0.1691	20.01 / 0.6526 / 0.1492
TL[38]+EU[46]	93.03	✓	✗	21.09 / 0.6682 / 0.1696	20.05 / 0.6267 / 0.1981	19.57 / 0.6079 / 0.2101	19.44 / 0.6027 / 0.2134	19.39 / 0.6002 / 0.2152
EU[46]+TL[38]	93.03	✓	✗	25.62 / 0.8339 / 0.0716	25.28 / 0.8290 / 0.0716	25.30 / 0.8300 / 0.0712	25.31 / 0.8306 / 0.0709	25.32 / 0.8306 / 0.0709
EU[46]+TR[15]	80.38	✓	EU,TR✓	19.02 / 0.6005 / 0.1612	19.41 / 0.6210 / 0.1564	19.64 / 0.6321 / 0.1536	19.72 / 0.6362 / 0.1527	19.77 / 0.6382 / 0.1522
Our	22.00	✓	✓	23.91 / 0.8091 / 0.0662	23.60 / 0.7973 / 0.0726	23.64 / 0.7964 / 0.0702	23.75 / 0.7971 / 0.0699	23.88 / 0.8074 / 0.0702

Table 2: Quantitative results (PSNR / SSIM / LPIPS) of the proposed framework and other methods on the Gev-RS simulated dataset. For supervised methods, TL refers to TimeLens[38], EU refers to EvUnRoll[46]. For the unsupervised method, TR refers to TimeReplayer[15]. LPIPS is calculated by the `lpipis` library[44] with AlexNet pretrained model[21]. ‘Event’ indicates whether events are used, and ‘SSL’ indicates whether it is self-supervised.

ERS-VFI. This camera outputs RGB frames with the resolution of  $3264 \times 2448$  and events with the resolution of  $1632 \times 1224$ . For all collected videos, 19 videos are selected for training, and 10 videos are for testing. Finally, 3630 and 2071 frames with aligned events are used as the training and testing sets, respectively. To prevent memory overflow during training, we apply data augmentation strategies of [5], such as random crop, to our ERS-VFI dataset for all compared methods.

### 5.1. Comparison with SoTA Methods

We compare our method with five SoTA methods under three VFI settings: (I) one SoTA event-guided VFI method—TimeLens (TL) [38], which is based on GS frames. (II) Combined methods, event-guided RS correction method—EvUnRoll(EU) [46] + event-guided VFI methods: TL[38] or TimeReplayer (TR) [15]. (III) Frame-based RS-to-GS VFI methods: CVR [8] and RSSR [5]. Except for the frame-based settings (III) which only takes RS frames, the inputs of (I) and (II) are both RS frames and events, and the ground truth frames of these three settings are the GS frames. **Evaluation on Gev-RS dataset:** Tab. 2 presents the quantitative results from  $4\times$  to  $32\times$  interpola-

tion, and the comparison of visual quality is shown in Fig. 6. Our method clearly outperforms the CVR and RSSR, which are frame-based RS-to-GS supervised VFI methods, in  $4\times$  interpolation by up to **1.32 dB** in PSNR. In addition, our method has the best LPIPS scores among all the compared methods (except  $8\times$  interpolation). Because our results do not suffer from the black holes, as shown in the red box of Fig. 6(g). This could be attributed to the capacity of estimating the complex non-linear motion of displacement field by utilizing the high temporal resolution of events. Without considering RS correction, the performances of TimeLens and the combination of TimeLens + EvUnroll degrade greatly with RS frames as inputs, and the interpolated results can not be recovered by RS correction methods.

Although the combination of two supervised methods—EvUnroll + TimeLens shows promising results owing to the high temporal resolution of events, such a two-step approach suffers from prohibitive computation costs (See Tab. 2). The performance of the combination of supervised method—EvUnroll + unsupervised method—TimeReplayer is limited, which demonstrates that the unsupervised VFI method can not be naively combined



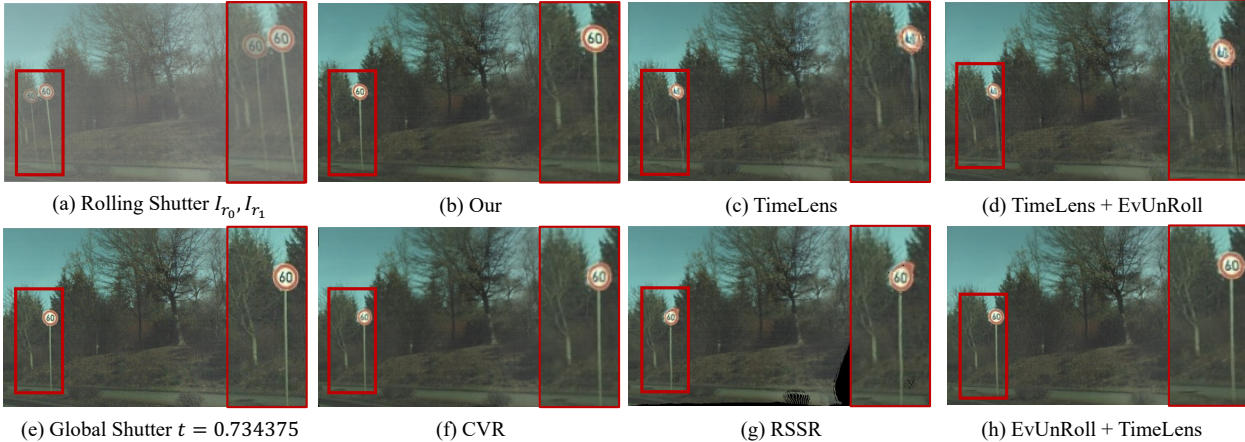


Figure 7: Visual comparison on Fastec-RS dataset.

Methods	Params(M)	Event	SSL	4×	8×	16×	24×	32×
CVR[8]	42.69	✗	✗	24.85 / 0.7538 / 0.1115	26.11 / 0.8003 / 0.1039	27.00 / 0.8330 / 0.0995	27.28 / 0.8434 / 0.0981	27.40 / 0.8481 / 0.0974
RSSR [5]	26.04	✗	✗	18.61 / 0.5975 / 0.1808	18.41 / 0.5844 / 0.1858	18.32 / 0.5780 / 0.1888	18.28 / 0.5759 / 0.1899	18.26 / 0.5747 / 0.1905
TL [38]	72.20	✓	✗	22.14 / 0.6334 / 0.1993	22.33 / 0.6408 / 0.1950	22.34 / 0.6413 / 0.1938	22.38 / 0.6425 / 0.1933	22.40 / 0.6432 / 0.1929
TL [38]+EU [46]	93.03	✓	✗	23.79 / 0.6739 / 0.1945	22.76 / 0.6376 / 0.2267	22.24 / 0.6182 / 0.2407	22.13 / 0.6141 / 0.2442	22.08 / 0.6120 / 0.2463
EU [46]+TL [38]	93.03	✓	✗	28.44 / 0.8450 / 0.0991	28.67 / 0.8487 / 0.0983	28.75 / 0.8504 / 0.0980	28.77 / 0.8507 / 0.0977	28.78 / 0.8510 / 0.0977
EU [46]+TR [15]	80.38	✓	EUX,TR✓	21.55 / 0.6149 / 0.1624	21.94 / 0.6318 / 0.1559	22.21 / 0.6431 / 0.1529	22.31 / 0.6478 / 0.1518	22.36 / 0.6499 / 0.1510
Our	22.00	✓	✓	26.27 / 0.8086 / 0.0834	26.29 / 0.8095 / 0.0827	26.26 / 0.8034 / 0.0810	26.37 / 0.8049 / 0.0853	26.31 / 0.8074 / 0.0836

Table 3: Quantitative results (PSNR / SSIM / LPIPS) of the proposed framework and other methods on the Fastec-RS[24] dataset.

with RS correction methods.

**Evaluation on Fastec-RS dataset** Here, we evaluate our methods on the Fastec-RS dataset, and the quantitative result is summarized in Tab. 3. We draw a similar conclusion as the experiments on the Gev-RS dataset, based on the quantitative comparison. Fig. 7 shows the visualization results of a outside street view captured by a moving camera and we have the sharpest reconstruction, for example, the number on the road sign (in the red box).

**Evaluation on ERS dataset** Fig. 1 shows the results of our method on the real-world dataset with 32× frame interpolation, and our method can generate successive smooth intermediate GS frames with spatialtemporal coherence, as shown in Fig. 1 (e). Also, Fig. 8 shows the GS frame (a) we reconstructed and the RS frame (b) we collected at time 0.25. By comparing the edge in the RS frames with that of events, we successfully correct the distorted edges, as shown in Fig.8 (a).

## 5.2. Ablation Studies

We conduct the following ablation experiments to evaluate the effectiveness of our proposed modules in Gev-RS dataset [46]: E-RAFT Channel, Time bins and iters of E-RAFT are set to 15, 6, and 12 in the baseline case which uses pretrained E-RAFT model [12]. **Loss function:** Tab.5

for each loss in Eq. 14. The 1st row represents the baseline, where solely the  $\mathcal{L}_{gs2rs}$  loss (Eq.10) is utilized, In the 2nd and 3rd rows, the displacement field loss (Eq.3) and RS-to-RS loss (Eq.13) are incorporated concurrently. As a result, increases are observed in the PSNR (+0.12) and SSIM (+0.0015). Also, when perceptual loss is added in our self-supervised setting (Tab. 4), we find it hard to obtain favorable outcomes.

**Time bins:** We conduct the experiments to evaluate the influences of different time bins on the displacement field estimation. As shown in Tab. 4 (row 1-4), the settings with six time bins obtains the best PSNR and SSIM score. The explanation is that when the number of time bins goes up, the 3D deformation field will be divided into more segments bringing better performance because of more capacity of the non-linear motion. However, an excessive number of time bins can result in accumulated errors of motion and the degradation of performance. Fig. 9 shows warp weights corresponding to GS at different times with six time bins. It can be observed that the nonlinear motion of the bus is estimated clearly.

**Perceptual loss:** Perceptual loss  $\mathcal{L}_p$  is widely used in previous work[15, 38, 18, 5, 8]. We also perform experiments to study the effectiveness of the perceptual loss [19] by applying the perpetual loss on GS-to-RS reconstruction and



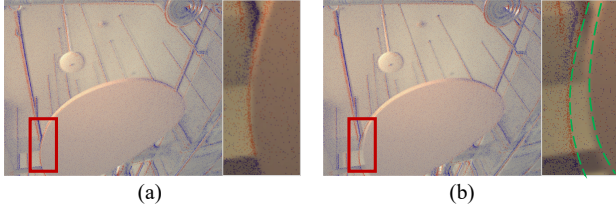


Figure 8: (a) The reconstructed GS frame with  $t = 0.25$  in real-world dataset and events around  $t = 0.25$ . (b) The RS frame and events around  $t = 0.25$ . The green lines mark the edge of events and the edge of the RS frame which has obvious distortion.

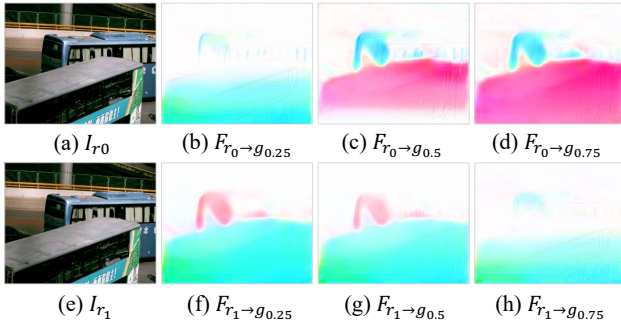


Figure 9: The rolling shutter frames (a) and (e) and warp weights visualization.  $F_{r_i \to g_t}$  means the warp weight from  $i$ -th RS frame to a GS frame at time  $t$ .

RS-to-RS warping. Tab. 4 (row 6-7) validates that introducing the perceptual loss can not boost the performance. Especially, applying perceptual loss only on the GS-to-RS reconstruction leads to the collapse of the displacement field and a worse performance. We argue that although the perceptual loss is applied in the compared method, it can not serve as the constraint in our self-supervised method.

**Pretrained optical flow model:** We evaluate the effect of the pre-train optical flow model by removing E-RAFT pre-train model. As shown in Tab. 4 (row 1,5), the experiments with pre-train E-RAFT model and without it demonstrate a similar performance. This indicates that our method is able to learn the optical flow without supervision.

**Sample points of Height and Time of Mask:** We investigate the impact of different sample points in height and time dimension during the estimation of the mask, as shown in Fig. 4. Tab. 4 (row 1,8-9) shows that the settings with different sample points have similar performance. This is because, for the setting with five height samples points and ten time samples points, each element has up to 50 samples points; thus, each element has ample samples to estimate the weight of warping.

**Model complexity:** Compared with other methods, our model stands out for its advantage in parameters and algorithmic complexity. Specifically, the parameter number of

	$T$	$P$	$\mathcal{L}_p$ GS-to-RS	$\mathcal{L}_p$ RS-to-RS	$S_h$	$S_t$	PSNR	SSIM
1	6	✓	✗	✗	50	100	23.91	0.8091
2	4	✓	✗	✗	50	100	23.78	0.8019
3	2	✓	✗	✗	50	100	23.32	0.7928
4	12	✓	✗	✗	50	100	23.67	0.7960
5	6	✗	✗	✗	50	100	23.88	0.8082
6	6	✓	✓	✗	50	100	18.50	0.6225
7	6	✓	✓	✓	50	100	23.84	0.8134
8	6	✓	✗	✗	5	10	23.90	0.8097
9	6	✓	✗	✗	100	200	24.00	0.8109

Table 4: Ablation result on Gev-RS.  $T$  indicates the count of time bins.  $P$  indicates the use of pre-train optical flow model.  $\mathcal{L}_p$  indicates the perceptual loss.  $S_h$  and  $S_t$  indicate the sample points for mask generation.

	$\mathcal{L}_{gs2rs}$	$\mathcal{L}_{field}$	$\mathcal{L}_{rs2rs}$	$\mathcal{L}_{gs}$	PSNR	SSIM
1	✓	✗	✗	✗	23.79	0.8076
2	✓	✓	✗	✗	23.91	0.8062
3	✓	✓	✓	✗	23.91	0.8091
4	✓	✓	✓	✓	<b>25.08</b>	<b>0.8319</b>

Table 5: Ablation of losses and supervised training for the  $4 \times$  interpolation on the Gev-RS dataset.

our framework is only one-fifth of EvUnRoll+TimeLens, as shown in Tab. 2. In addition, during the inference stage, our approach only needs to estimate DF once for generating all GS frames. In contrast, TimeLen and TimeReplayer require individual calculation of optical flow for each frame causing high computation cost.

## 6. Conclusion

In conclusion, this paper addressed the limitations of previous VFI methods by proposing a novel approach that considers the rolling shutter pattern commonly used in video capture. We introduced the displacement field that can effectively use the high temporal resolution property of events and model non-linear motion. Based on the displacement field, our framework realizes arbitrary frame rate VFI (*e.g.* 32 $\times$ ) as well as the reciprocal reconstruction between RS and GS frames in a self-supervised learning. We also employ two simulated datasets and collect a real-world dataset with spatially aligned events and RS RGB frames to support our cycle training. Experiments demonstrate the effectiveness of our method, both qualitatively and quantitatively.

**Limitation and Future Work** As the first attempt to employ a self-supervised approach for VFI based on RS images and events, our study has yielded promising results on simulated data. However, in the absence of quantitative metrics on real-world data, the efficacy of our method remains to be fully evaluated. In light of this limitation, future research should establish collaborations with camera

manufacturers to capture simultaneous RS, GS, and events, thereby enabling robust and comprehensive evaluations for the development of innovative techniques for applications.

## References

- [1] Mingdeng Cao, Zhihang Zhong, Jiahao Wang, Yinqiang Zheng, and Yujiu Yang. Learning adaptive warping for real-world rolling shutter correction. In *Proceedings of the IEEE/CVF Conference on Computer Vision and Pattern Recognition*, pages 17785–17793, 2022. 3
- [2] Zhixiang Chi, Rasoul Mohammadi Nasiri, Zheng Liu, Juwei Lu, Jin Tang, and Konstantinos N Plataniotis. All at once: Temporally adaptive multi-frame interpolation with advanced motion modeling. In *European Conference on Computer Vision*, pages 107–123. Springer, 2020. 2, 3
- [3] Jung-Bum Chun, Hunjoon Jung, and Chong-Min Kyung. Suppressing rolling-shutter distortion of cmos image sensors by motion vector detection. *IEEE Transactions on Consumer Electronics*, 54(4):1479–1487, 2008. 1
- [4] Jiong Dong, Kaoru Ota, and Mianxiong Dong. Video frame interpolation: A comprehensive survey. *ACM Transactions on Multimedia Computing, Communications and Applications*, 2022. 2
- [5] Bin Fan and Yuchao Dai. Inverting a rolling shutter camera: bring rolling shutter images to high framerate global shutter video. In *Proceedings of the IEEE/CVF International Conference on Computer Vision*, pages 4228–4237, 2021. 2, 3, 4, 7, 8
- [6] Bin Fan and Yuchao Dai. Inverting a rolling shutter camera: Bring rolling shutter images to high framerate global shutter video. *2021 IEEE/CVF International Conference on Computer Vision (ICCV)*, pages 4208–4217, 2021. 3
- [7] Bin Fan, Yuchao Dai, and Mingyi He. Sunet: Symmetric undistortion network for rolling shutter correction. *2021 IEEE/CVF International Conference on Computer Vision (ICCV)*, pages 4521–4530, 2021. 3
- [8] Bin Fan, Yuchao Dai, Zhiyuan Zhang, Qi Liu, and Mingyi He. Context-aware video reconstruction for rolling shutter cameras. In *Proceedings of the IEEE/CVF Conference on Computer Vision and Pattern Recognition*, pages 17572–17582, 2022. 1, 2, 3, 4, 6, 7, 8
- [9] Guillermo Gallego, Tobi Delbrück, Garrick Orchard, Chiara Bartolozzi, Brian Taba, Andrea Censi, Stefan Leutenegger, Andrew J Davison, Jörg Conrath, Kostas Daniilidis, et al. Event-based vision: A survey. *IEEE transactions on pattern analysis and machine intelligence*, 44(1):154–180, 2020. 2
- [10] Daniel Gehrig, Mathias Gehrig, Javier Hidalgo-Carrió, and Davide Scaramuzza. Video to events: Recycling video datasets for event cameras. In *Proceedings of the IEEE/CVF Conference on Computer Vision and Pattern Recognition*, pages 3586–3595, 2020. 6
- [11] Daniel Gehrig, Antonio Loquercio, Konstantinos G Derpanis, and Davide Scaramuzza. End-to-end learning of representations for asynchronous event-based data. In *Proceedings of the IEEE/CVF International Conference on Computer Vision*, pages 5633–5643, 2019. 2
- [12] Mathias Gehrig, Mario Millhäusler, Daniel Gehrig, and Davide Scaramuzza. E-raft: Dense optical flow from event cameras. In *2021 International Conference on 3D Vision (3DV)*, pages 197–206. IEEE, 2021. 2, 4, 8
- [13] Chris A Glasbey and Kantilal Vardichand Mardia. A review of image-warping methods. *Journal of applied statistics*, 25(2):155–171, 1998. 5
- [14] Akash Gupta, Sudhir Kumar Singh, and Amit K Roy-Chowdhury. Joint video rolling shutter correction and super-resolution. In *Proceedings of the IEEE/CVF Winter Conference on Applications of Computer Vision*, pages 4946–4955, 2023. 2
- [15] Weihua He, Kaichao You, Zhendong Qiao, Xu Jia, Ziyang Zhang, Wenhui Wang, Huchuan Lu, Yaoyuan Wang, and Jianxing Liao. Timereplayer: Unlocking the potential of event cameras for video interpolation. In *Proceedings of the IEEE/CVF Conference on Computer Vision and Pattern Recognition*, pages 17804–17813, 2022. 2, 3, 5, 7, 8
- [16] Johan Hedborg, Per-Erik Forssén, Michael Felsberg, and Erik Ringaby. Rolling shutter bundle adjustment. In *2012 IEEE Conference on Computer Vision and Pattern Recognition*, pages 1434–1441. IEEE, 2012. 1
- [17] Alain Hore and Djemel Ziou. Image quality metrics: Psnr vs. ssim. In *2010 20th international conference on pattern recognition*, pages 2366–2369. IEEE, 2010. 6
- [18] Huaizu Jiang, Deqing Sun, Varun Jampani, Ming-Hsuan Yang, Erik Learned-Miller, and Jan Kautz. Super slo-mo: High quality estimation of multiple intermediate frames for video interpolation. In *Proceedings of the IEEE conference on computer vision and pattern recognition*, pages 9000–9008, 2018. 2, 3, 5, 8
- [19] Justin Johnson, Alexandre Alahi, and Li Fei-Fei. Perceptual losses for real-time style transfer and super-

- resolution. In *Computer Vision—ECCV 2016: 14th European Conference, Amsterdam, The Netherlands, October 11-14, 2016, Proceedings, Part II 14*, pages 694–711. Springer, 2016. 8
- [20] Diederik P Kingma and Jimmy Ba. Adam: A method for stochastic optimization. *arXiv preprint arXiv:1412.6980*, 2014. 6
- [21] Alex Krizhevsky, Ilya Sutskever, and Geoffrey E Hinton. Imagenet classification with deep convolutional neural networks. *Communications of the ACM*, 60(6):84–90, 2017. 7
- [22] Wei-Sheng Lai, Jia-Bin Huang, Narendra Ahuja, and Ming-Hsuan Yang. Fast and accurate image super-resolution with deep laplacian pyramid networks. *IEEE transactions on pattern analysis and machine intelligence*, 41(11):2599–2613, 2018. 6
- [23] Yizhen Lao and Omar Ait-Aider. A robust method for strong rolling shutter effects correction using lines with automatic feature selection. In *Proceedings of the IEEE Conference on Computer Vision and Pattern Recognition*, pages 4795–4803, 2018. 2
- [24] Peidong Liu, Zhaopeng Cui, Viktor Larsson, and Marc Pollefeys. Deep shutter unrolling network. *2020 IEEE/CVF Conference on Computer Vision and Pattern Recognition (CVPR)*, pages 5940–5948, 2020. 2, 3, 6, 8
- [25] Simone Meyer, Abdelaziz Djelouah, Brian McWilliams, Alexander Sorkine-Hornung, Markus Gross, and Christopher Schroers. Phasenet for video frame interpolation. In *Proceedings of the IEEE Conference on Computer Vision and Pattern Recognition*, pages 498–507, 2018. 2, 3
- [26] Eyal Naor, Itai Antebi, Shai Bagon, and Michal Irani. Combining internal and external constraints for unrolling shutter in videos. In *European Conference on Computer Vision*, pages 119–134. Springer, 2022. 2
- [27] Simon Niklaus and Feng Liu. Context-aware synthesis for video frame interpolation. In *Proceedings of the IEEE conference on computer vision and pattern recognition*, pages 1701–1710, 2018. 2, 3
- [28] Simon Niklaus and Feng Liu. Softmax splatting for video frame interpolation. In *Proceedings of the IEEE/CVF Conference on Computer Vision and Pattern Recognition*, pages 5437–5446, 2020. 2, 3
- [29] Genady Paikin, Yotam Ater, Roy Shaul, and Evgeny Soloveichik. Efi-net: Video frame interpolation from fusion of events and frames. In *Proceedings of the IEEE/CVF Conference on Computer Vision and Pattern Recognition*, pages 1291–1301, 2021. 2, 3
- [30] Avinash Paliwal and Nima Khademi Kalantari. Deep slow motion video reconstruction with hybrid imaging system. *IEEE transactions on pattern analysis and machine intelligence*, 42(7):1557–1569, 2020. 2, 3
- [31] Anil Singh Parihar, Disha Varshney, Kshitija Pandya, and Ashray Aggarwal. A comprehensive survey on video frame interpolation techniques. *The Visual Computer*, pages 1–25, 2022. 2
- [32] Junheum Park, Keunsoo Ko, Chul Lee, and Chang-Su Kim. Bmbc: Bilateral motion estimation with bilateral cost volume for video interpolation. In *European Conference on Computer Vision*, pages 109–125. Springer, 2020. 2, 3
- [33] Henri Rebecq, Guillermo Gallego, Elias Mueggler, and Davide Scaramuzza. Emvs: Event-based multi-view stereo—3d reconstruction with an event camera in real-time. *International Journal of Computer Vision*, 126(12):1394–1414, 2018. 2, 4
- [34] Vijay Rengarajan, Amba Mudram N Rajagopalan, and Rangarajan Aravind. From bows to arrows: Rolling shutter rectification of urban scenes. In *Proceedings of the IEEE Conference on Computer Vision and Pattern Recognition*, pages 2773–2781, 2016. 2
- [35] Cedric Scheerlinck, Henri Rebecq, Timo Stoffregen, Nick Barnes, Robert Mahony, and Davide Scaramuzza. Ced: Color event camera dataset. In *Proceedings of the IEEE/CVF Conference on Computer Vision and Pattern Recognition Workshops*, pages 0–0, 2019. 2, 6
- [36] David Schubert, Nikolaus Demmel, Lukas von Stumberg, Vladyslav Usenko, and Daniel Cremers. Rolling-shutter modelling for direct visual-inertial odometry. In *2019 IEEE/RSJ International Conference on Intelligent Robots and Systems (IROS)*, pages 2462–2469. IEEE, 2019. 1
- [37] Stepan Tulyakov, Alfredo Bochicchio, Daniel Gehrig, Stamatios Georgoulis, Yuanyou Li, and Davide Scaramuzza. Time lens++: Event-based frame interpolation with parametric non-linear flow and multi-scale fusion. In *Proceedings of the IEEE/CVF Conference on Computer Vision and Pattern Recognition*, pages 17755–17764, 2022. 2, 3
- [38] Stepan Tulyakov, Daniel Gehrig, Stamatios Georgoulis, Julius Erbach, Mathias Gehrig, Yuanyou Li, and Davide Scaramuzza. Time lens: Event-based video frame interpolation. In *Proceedings of the IEEE/CVF Conference on Computer Vision and Pattern Recognition*, pages 16155–16164, 2021. 2, 3, 7, 8
- [39] Lin Wang, Tae-Kyun Kim, and Kuk-Jin Yoon. Eventsr: From asynchronous events to image reconstruction, restoration, and super-resolution via end-to-end adversarial learning. In *Proceedings of the*

*IEEE/CVF Conference on Computer Vision and Pattern Recognition*, pages 8315–8325, 2020. 4

- [40] Zhou Wang, Alan C Bovik, Hamid R Sheikh, and Eero P Simoncelli. Image quality assessment: from error visibility to structural similarity. *IEEE transactions on image processing*, 13(4):600–612, 2004. 6
- [41] Song Wu, Kaichao You, Weihua He, Chen Yang, Yang Tian, Yaoyuan Wang, Ziyang Zhang, and Jianxing Liao. Video interpolation by event-driven anisotropic adjustment of optical flow. In *Computer Vision—ECCV 2022: 17th European Conference, Tel Aviv, Israel, October 23–27, 2022, Proceedings, Part VII*, pages 267–283. Springer, 2022. 2, 3
- [42] Xiangyu Xu, Li Siyao, Wenxiu Sun, Qian Yin, and Ming-Hsuan Yang. Quadratic video interpolation. *Advances in Neural Information Processing Systems*, 32, 2019. 2, 3
- [43] Zhiyang Yu, Yu Zhang, Deyuan Liu, Dongqing Zou, Xijun Chen, Yebin Liu, and Jimmy S Ren. Training weakly supervised video frame interpolation with events. In *Proceedings of the IEEE/CVF International Conference on Computer Vision*, pages 14589–14598, 2021. 2, 3
- [44] Richard Zhang, Phillip Isola, Alexei A Efros, Eli Shechtman, and Oliver Wang. The unreasonable effectiveness of deep features as a perceptual metric. In *CVPR*, 2018. 6, 7
- [45] Xu Zheng, Yexin Liu, Yunfan Lu, Tongyan Hua, Tianbo Pan, Weiming Zhang, Dacheng Tao, and Lin Wang. Deep learning for event-based vision: A comprehensive survey and benchmarks. *arXiv preprint arXiv:2302.08890*, 2023. 2
- [46] Xinyu Zhou, Peiqi Duan, Yi Ma, and Boxin Shi. Evunroll: Neuromorphic events based rolling shutter image correction. In *Proceedings of the IEEE/CVF Conference on Computer Vision and Pattern Recognition*, pages 17775–17784, 2022. 2, 3, 6, 7, 8
- [47] Bingbing Zhuang, Quoc-Huy Tran, Pan Ji, Loong-Fah Cheong, and Manmohan Chandraker. Learning structure-and-motion-aware rolling shutter correction. In *Proceedings of the IEEE/CVF Conference on Computer Vision and Pattern Recognition*, pages 4551–4560, 2019. 2